

Exploring a quantum-information-relevant magnonic material: Ultralow damping at low temperature in the organic ferrimagnet $V[TCNE]_x$

Cite as: AVS Quantum Sci. **3**, 026801 (2021); doi: 10.1116/5.0044193

Submitted: 14 January 2021 · Accepted: 25 May 2021 ·

Published Online: 21 June 2021



View Online



Export Citation



CrossMark

H. Yusuf,^{1,a)} M. Chilcote,^{1,2} D. R. Candido,³ S. Kurfman,¹ D. S. Cormode,¹ Y. Lu,¹ M. E. Flatté,³ and E. Johnston-Halperin¹

AFFILIATIONS

¹Department of Physics, The Ohio State University, Columbus, Ohio 43210

²School of Applied and Engineering Physics, Cornell University, Ithaca, New York 14853

³Department of Physics and Astronomy, University of Iowa, Iowa City, Iowa, 52242

^{a)}Electronic mail: yusuf.69@osu.edu

ABSTRACT

Quantum information science and engineering require novel low-loss magnetic materials for magnon-based quantum-coherent operations. The search for low-loss magnetic materials, traditionally driven by applications in microwave electronics near room temperature, has gained additional constraints from the need to operate at cryogenic temperatures for many applications in quantum information science and technology. Whereas yttrium iron garnet (YIG) has been the material of choice for decades, the emergence of molecule-based materials with robust magnetism and ultra-low damping has opened new avenues for exploration. Specifically, thin films of vanadium tetracyanoethylene ($V[TCNE]_x$) can be patterned into the multiple, connected structures needed for hybrid quantum elements and have shown room-temperature Gilbert damping ($\alpha = 4 \times 10^{-5}$) that rivals the intrinsic (bulk) damping otherwise seen only in highly polished YIG spheres (far more challenging to integrate into arrays). Here, the authors present a comprehensive and systematic study of the low-temperature magnetization dynamics for $V[TCNE]_x$ thin films, with implications for their application in quantum systems. These studies reveal a temperature-driven, strain-dependent magnetic anisotropy that compensates the thin-film shape anisotropy and the recovery of a magnetic resonance linewidth at 5 K that is comparable to room-temperature values (roughly 2 G at 9.4 GHz). The authors can account for these variations of the $V[TCNE]_x$ linewidth within the context of scattering from very dilute paramagnetic impurities and anticipate additional linewidth narrowing as the temperature is further reduced.

Published under an exclusive license by AIP Publishing. <https://doi.org/10.1116/5.0044193>

The search for low-loss magnetic materials dates to the early days of radio and microwave electronics,^{1–3} and the study of elementary excitations, or magnons, in these magnetically ordered materials has proven to be a rich area of research for both fundamental physics and their potential technological applications. More recently, interest in these low-loss systems has expanded to include applications in the field of quantum information technology such as quantum sensing and quantum transduction,^{4–7} wherein low-temperature operation allows for the freeze-out of thermal excitations and access to the single-quantum regime. In this regime, the field of quantum magnonics utilizes hybrid architectures for coupling magnons to other quantum degrees of freedom, such as microwave photons, with the aim of extending their functionality to the quantum limit.^{8,9} It has been demonstrated that magnons can be resonantly excited over a

wide range of microwave frequencies, allowing for precise control of qubit states mediated by coherent exchange via cavity-mode photon excitations.^{4,7} Magnons also exhibit the potential to coherently couple localized spin qubits with high cooperativity.¹⁰ However, while magnons exist in a wide range of materials, the same delocalized electrons that are most often responsible for stabilizing a ferromagnetic order also contribute to electron–magnon scattering,¹¹ leading to substantial losses in most metallic ferromagnets. As a result, the study of low-dissipation magnon dynamics for quantum applications has focused on insulating ferromagnets and ferrimagnets, with yttrium iron garnet (YIG) and its close relatives holding pride of place as the benchmark low-loss materials for more than 50 years.^{4,12–14} As a result, despite these long-standing and emerging needs, applications are still constrained by the material limitations of YIG, namely, the need for

growth or annealing at high temperatures (typically 800 °C)^{15–17} and the resulting difficulty in integrating and patterning YIG thin-films with other microwave electronic structures and devices.

In this context, the emergence of the molecule-based ferrimagnet vanadium tetracyanoethylene (V[TCNE]_x) has dramatically expanded the playing field for low-loss magnets. Despite what one might expect from its molecular building blocks, V[TCNE]_x has a magnetic ordering temperature of over 600 K and shows sharp hysteresis at room temperature.^{18–20} Moreover, its dynamic properties are exceptional, showing an ultranarrow ferromagnetic resonance (FMR) linewidth (typically ~1–1.5 G at 9.4 GHz) with a Gilbert damping parameter, α , of 4×10^{-5} for thin-films.^{18,21} As a comparison, the best YIG thin-films typically show $\alpha = 6.5 \times 10^{-5}$ (Ref. 22), and a value of 4×10^{-5} is competitive with the intrinsic damping of bulk YIG $\alpha = 3 \times 10^{-5}$.^{15,23} From an application perspective, V[TCNE]_x has been shown to deposit on a wide variety of substrates without compromising material quality,^{24–26} facile encapsulation allows for direct integration with pre-patterned microwave structures for operation under ambient conditions,²⁷ and recent work has demonstrated patterning at length scales down to 10 μm without increased damping.²¹ However, while these properties clearly establish the potential of V[TCNE]_x for new applications in traditional microwave electronics, very little is known about its low-temperature magnetization dynamics and therefore its potential for applications in quantum information science and engineering (QISE).

Here, we present a detailed study of the low-temperature magnetic resonance of V[TCNE]_x films. We identify two regimes. In the high-temperature regime, extending from 300 K down to 9 K, we observe a monotonic shift in the resonance frequency consistent with a temperature-dependent strain. This strain results in a crystal-field anisotropy that increases with decreasing temperature with a magnitude of at least 140 Oe and the same symmetry, but opposite sign, to the shape anisotropy of the thin-film. In addition, we observe an increase in the linewidth consistent with magnon scattering from paramagnetic impurities similar to what has been observed in YIG,^{23,28,29} but with an amplitude three times smaller (i.e., an increase in linewidth by nine times in V[TCNE]_x as compared to 28 times in YIG^{23,30}). In the low-temperature regime, starting at 9 K and extending to 5 K, we observe a discontinuous change in both anisotropy and linewidth; the anisotropy abruptly reverts to the room-temperature symmetry (in-plane easy-axis), and the linewidth approaches room-temperature values (2.58 G) at 5 K. This linewidth variation can be explained using a model for scattering between magnons and paramagnetic impurities that takes into account the finite spin lifetime of the impurity spins.^{23,31} At high temperatures (above 100 K), the spin lifetime is sufficiently short that changes in temperature do not lead to significant changes in scattering rate, and at low temperatures (below 9 K), the spin lifetime becomes long with respect to the spin-magnon scattering time, resulting in a saturation of the excited state. At intermediate temperatures (from 9 K to 100 K), this spin-magnon scattering dominates relaxation due to the increase in the ground state impurity population, which results in a local maximum in the linewidth that is nine times larger than the room-temperature value. These results are extremely promising for low-temperature applications of V[TCNE]_x magnonics, promising low-temperature magnon resonators with unprecedented low loss that can be integrated on-chip into microwave electronic circuits and devices.^{20,21}

For this study, thin films of V[TCNE]_x are deposited on sapphire [Al₂O₃ (0001)] substrates using a chemical vapor deposition (CVD) growth process consistent with prior reports.^{18,19} Briefly, argon gas transfers the two precursors tetracyanoethylene (TCNE) and vanadium hexacarbonyl [V(CO)₆] into the reaction zone of a custom-built CVD reactor [Fig. 1(a)] where V[TCNE]_x is deposited onto polished sapphire substrates. The system is temperature controlled to maintain the TCNE, V(CO)₆ and the reaction zones at 65 °C, 10 °C, and 50 °C, respectively. After growth, the sample is mounted on a custom, microwave-compatible sample holder and sealed using a septa cap in an electron paramagnetic resonance (EPR) grade quartz tube in an argon environment. When the sample is not being measured, it is stored in a –35 °C freezer housed in an argon glovebox and is stable for over one month.²⁷

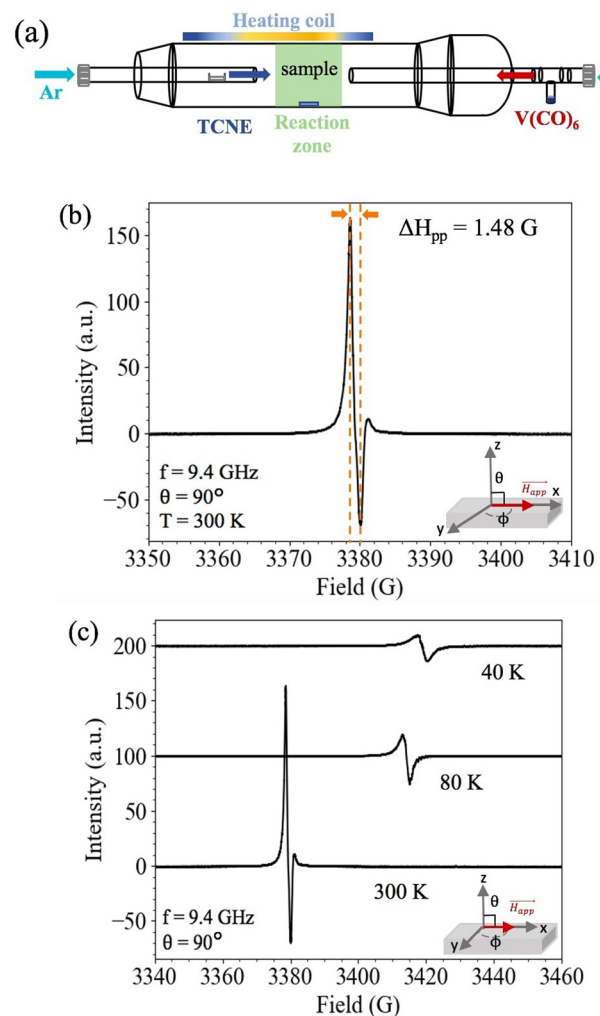


Fig. 1. (a) Schematic (planar view) of the CVD growth system; (b) FMR scan of the V[TCNE]_x thin film at 300 K with the applied magnetic field applied in the plane (IP) of the sample with $\theta = 90^\circ$ and resonance frequency of 9.4 GHz. ΔH_{pp} denotes the peak-to-peak linewidth measured as the difference between the positive and negative peak positions; (c) FMR line scans for in-plane field orientation at 300 K, 80 K, and 40 K with $\theta = 90^\circ$ and resonance frequency of 9.4 GHz.

Ferromagnetic resonance (FMR) measurements are performed using a Bruker EMX Plus X-band EPR spectrometer at temperatures ranging from 300 K down to 5 K. The microwave frequency of the spectrometer is tuned between 9 and 10 GHz for optimal microwave cavity performance before the measurement, and then the frequency is fixed while the DC field is swept during data collection. Figure 1(b) shows a representative room-temperature FMR measurement of a typical V[TCNE]_x thin-film with the external magnetic field applied in the plane of the sample. The resonance feature is consistent with previously reported high-quality V[TCNE]_x thin-film growth, showing a peak-to-peak linewidth of 1.5 G at 9.4 GHz.^{18,19}

Comparing these data to FMR measurements at temperatures of 80 K and 40 K [Fig. 1(c)] shows an increase in the resonance field of over 40 G (roughly half of the saturation magnetization, $4\pi M_s$) as the temperature decreases. Since the applied microwave frequency is held constant at 9.4 GHz, this shift must arise from fields internal to the V[TCNE]_x film, i.e., magnetic anisotropy fields. Note that since the value of the DC applied field varies between 3350 and 3450 G, well above $4\pi M_s$, changes in the magnetization of the film are not expected to contribute to this field shift. In a similar fashion, changes in the shape-dependent anisotropy fields can be ruled out, leaving only changes to the crystal-field anisotropy as a potential source of this phenomenon. Crystal-field anisotropy originates from the interaction of a material's mean exchange field and the angular momenta of neighboring atoms (ions) in the material, indicating that there is a temperature dependence to the local atomic environment within the V[TCNE]_x films, e.g., due to a temperature-dependent strain within the film.

In order to more comprehensively map out this phenomenon, angle dependent FMR measurements are performed to quantitatively track changes in the magnetic anisotropy at temperatures of 300 K, 80 K, and 40 K (Fig. 2). Variation of the magnetic resonance field as a function of the angle between the applied field and the principal axes of the film can be modeled by considering the free energy of the magnetic system with anisotropic contributions. If we consider the case of a uniaxial anisotropy with the hard axis perpendicular to the easy axis and where the magnetization is parallel to the external field (i.e., external field is much larger than the saturation magnetization, as is the case here), the total magnetostatic energy is as follows:³²

$$E = -\mathbf{M} \cdot \mathbf{H} + 2\pi(\mathbf{M} \cdot \mathbf{n})^2 - K(\mathbf{M} \cdot \mathbf{u}/M)^2, \quad (1)$$

where \mathbf{M} is the magnetization, \mathbf{H} is the applied magnetic field, \mathbf{n} is the unit vector parallel to the normal of the magnetic sample, \mathbf{u} is the unit vector parallel to the easy axis, and K is an anisotropy constant. For the case of in-plane uniaxial anisotropy, this simplifies to

$$E = -MH(\sin\phi\sin^2\theta + \cos^2\theta) + 2\pi M^2\cos^2\theta - K\sin^2\theta\sin\phi^2, \quad (2)$$

where θ is the angle between \mathbf{M} and the sample normal and ϕ is the azimuthal angle. Minimizing the magnetostatic energy with respect to θ , one will find that the easy-axis orientation occurs when $\theta = 2n\pi \pm \frac{\pi}{2}$, where n is an integer. Using this simple symmetry analysis, we can see that the data in Fig. 2 indicate that the easy axis lies in-plane at a temperature of 300 K (i.e., the resonance field is smallest when the applied magnetic field lies in-plane) and out-of-plane at a temperature of 40 K (i.e., the resonance field is smallest when the applied magnetic field is out-of-plane). In this context, the lack of variation in resonance field at 80 K indicates a nearly isotropic magnetic response. This switch

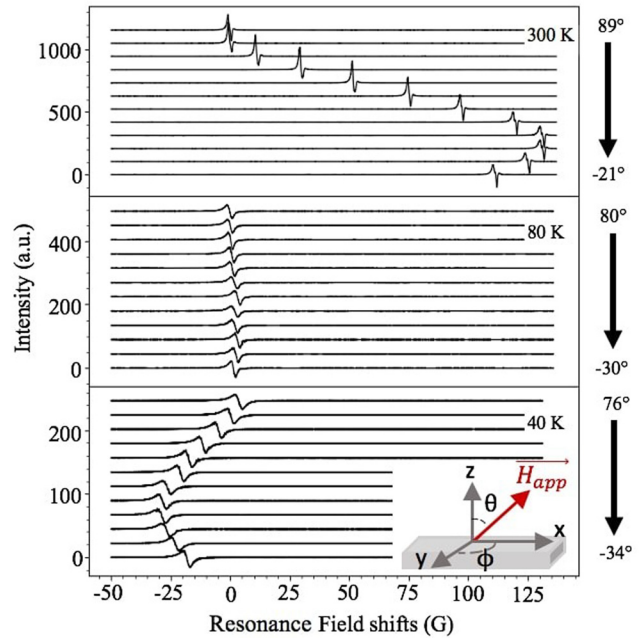


Fig. 2. Angle-dependent FMR spectra at temperatures of 300 K, 80 K, and 40 K at different field orientations with respect to the sample normal. Nominally, the sample is rotated from $\theta = -10^\circ$ to $\theta = 100^\circ$ in increments of 10° , where $\theta = 90^\circ$ and $\theta = 0^\circ$ are in-plane and out-of-plane field orientations, respectively. Angle corrections have been taken into account [through fitting with Eq. (3)] to reflect the actual rotation angles, denoted by the black arrows to the right of each of the temperature-labeled panels.

in magnetic easy-axis from in-plane to out-of-plane further supports the proposition that there is an additional temperature-dependent crystal-field contribution to the magnetic anisotropy.

In previous studies, templated growth of V[TCNE]_x resulting in nanowire morphologies induced an additional in-plane magnetic anisotropy with easy axis perpendicular to the long axis of the nanowires, strongly suggesting the presence of a strain-dependent contribution to the crystal-field anisotropy.³³ In the thin films studied here, such a strain-dependent crystal-field effect would be expected to generate anisotropy parallel to the surface normal, i.e., in the out-of-plane direction. The anisotropy field would then be parallel to the expected shape anisotropy from a thin film, though not necessarily with the same sign. As a result, if there is a difference in the coefficient of thermal expansion between the V[TCNE]_x film and the sapphire substrate then the temperature dependence of magnetic anisotropy can potentially be understood as a proxy for a temperature dependence of strain in the thin film; such variations in strain lead to changes in the local atomic structure, leading to the observed changes in magnetic anisotropy. We note that while the coefficient of thermal expansion for V[TCNE]_x has not yet been measured, the value for sapphire is 5.4 ppm/K and typical values for molecular-based solids can range somewhere between 28 and 500 ppm/K.³⁴ Assuming no strain at room temperature, this would then imply a compressive strain between 0.67% and 15% at the sapphire-V[TCNE]_x interface at 5 K, leading to an out-of-plane distortion whose symmetry is consistent with the observed anisotropy.

A schematic describing how these two anisotropy fields would be expected to interact as a function of temperature can be found in Fig. 3(a). At a temperature of 300 K [Fig. 3(a), upper panels], the orientation of the easy axis is determined by the shape anisotropy, resulting in an in-plane easy axis for thin films. However at a temperature of 40 K [Fig. 3(a) lower panels], there is an additional crystal-field anisotropy, H_{\perp} , proposed that dominates the shape anisotropy, reorienting the easy axis to be out-of-plane. This symmetry analysis also explains the lack of orientation dependence at a temperature of 80 K, which is apparently the temperature at which the strain-driven crystal-field anisotropy perfectly cancels out the shape anisotropy. We note that similar phenomenology is also observed in vanadium methyl tricyanoethylenecarboxylate (V[MeTCEC]_x) thin films (see the [supplementary material](#)) indicating that this temperature- and strain-dependent anisotropy is a general property of this class of metal-ligand ferrimagnets.

The fact that the shape and proposed crystal-field anisotropies have the same symmetry makes it challenging to distinguish between the two; therefore, an effective field is defined as $H_{eff} = 4\pi M_{eff} = 4\pi M_s - H_{\perp}$, where M_s is the saturation magnetization and H_{\perp} is the crystal-field anisotropy. Figure 2 shows the effects of this net anisotropy field in the form of resonance field shifts and a change in the easy-axis orientation. Quantitatively extracting the magnitude and direction of this anisotropy field provides detailed insight into the role of crystal-field anisotropy in tuning the magnetic response of V[TCNE]_x thin-films. To this end, each scan is fit to the sum of the derivatives of absorption and dispersion from a Lorentzian function to extract the resonance frequency and linewidth (experimental data are obtained using a modulated-field technique that yields the derivative of the expected Lorentzian resonance line shape). For scans showing an out-of-plane easy axis, a single derivative sum provides good agreement with the data, while for scans showing in-plane easy axis, a more complex structure is observed requiring the addition of up to three derivative sums. In the results discussed below, we focus on the behavior of the primary, i.e., largest amplitude, peak (a full description of the fitting and resulting phenomenology can be found in the [supplementary material](#)).

Figure 3(b) shows the extracted resonance field plotted against sample rotation angle for the high- and low-temperature data shown in Fig. 2, 300 K and 40 K, respectively. Taking into account a uniaxial out-of-plane anisotropy defined by H_{eff} , as described above, the angular dependence for in-plane to out-of-plane rotation of a thin film sample is given by^{19,35,36}

$$\frac{\omega}{\gamma} = \sqrt{(H - H_{eff} \cos^2 \theta)(H - H_{eff} \cos 2\theta)} = \sqrt{(H - (4\pi M_s - H_{\perp}) \cos^2 \theta)(H - (4\pi M_s - H_{\perp}) \cos 2\theta)}, \quad (3)$$

where ω is the resonance frequency and γ is the gyromagnetic ratio. As a result, the phenomenology of the data presented in Fig. 2 can be understood as an H_{eff} that is positive at 300 K and negative at 40 K, as H_{\perp} increases with decreasing temperature, consistent with the mechanism for anisotropy switching described in Fig. 3(a). This qualitative understanding can be made quantitative by fitting the data in Fig. 2 using Eq. (3) to extract $H_{eff} = 4\pi M_{eff}$ of 91.2 ± 1.6 G and -22.8 ± 0.4 G, respectively.

Figure 3(c) shows this H_{eff} plotted against temperature over the temperature range from 300 K to 5 K, extracted from angular

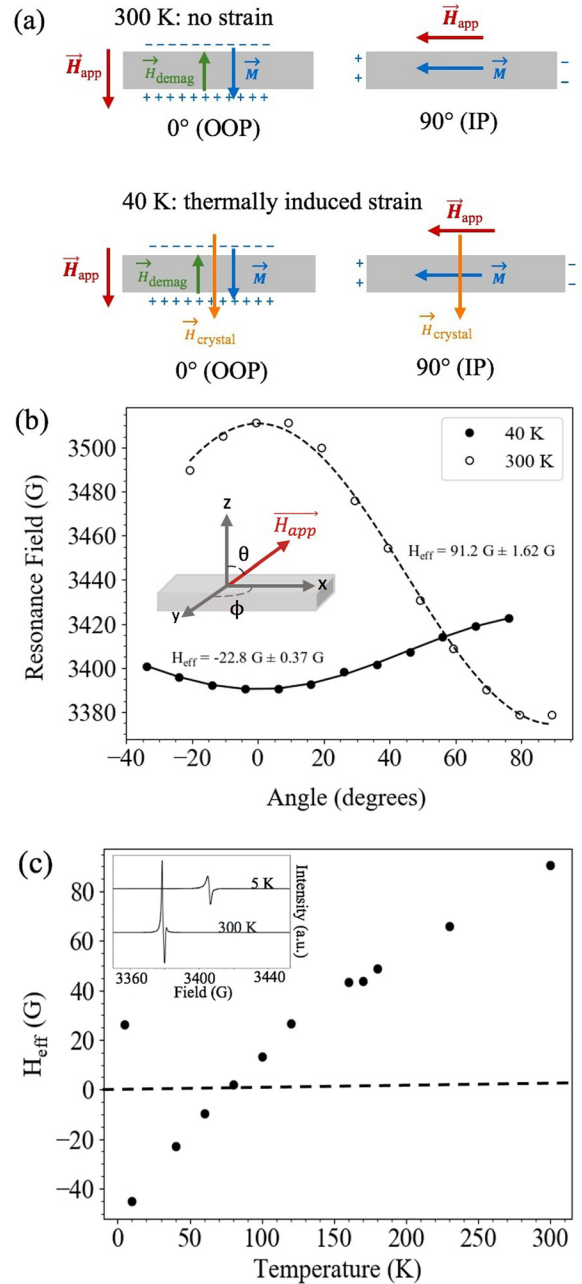


Fig. 3. (a) Schematic of the changes in anisotropy at 300 K and 40 K. \vec{H}_{app} denotes the external magnetic field, \vec{H}_{demag} represents the demagnetizing field of the V[TCNE]_x film, and $\vec{H}_{crystal}$ is the crystal-field anisotropy. It should be noted that a finite thin film has a (negligibly) small demagnetization field when the external field is applied in the plane since this is not a truly infinite film; (b) resonance field at different field orientations plotted against sample rotation angles for 300 K (open circles) to 40 K (filled circles) and fits to Eq. (3) (dashed and solid line, respectively) to extract the effective field H_{eff} ; (c) H_{eff} plotted against temperature ranging from 300 K to 5 K. The inset shows the FMR lineshapes at 300 K and 5 K; fitting the data to extract the linewidth at FWHM gives 1.63 and 2.58 G, respectively; this shows that the two linewidths are indeed comparable with the linewidth at 5 K only about 1.66 times larger than the room-temperature value. For both (b) and (c), experimental errors are smaller than the point size.

dependencies such as the measurements presented in Fig. 2. It should be noted that each anisotropy point in Fig. 3(c) represents a fit to a complete angular dependence such as the data shown in Fig. 3(b). The effective field makes a smooth transition through zero from positive (in-plane) to negative (out-of-plane) at a temperature of roughly 80 K. This behavior is qualitatively consistent with the phenomenological model presented above and reveals a magnitude of the variation in H_{eff} , from $+91.2 \pm 1.6$ G at 300 K to -45.2 ± 1.1 G at 10 K that is roughly 150% of the room-temperature value.

Notably, this more comprehensive study also reveals new phenomenology at the lowest temperature of 5 K, where the anisotropy abruptly shifts back to in-plane with a value of $+26.2 \pm 0.6$ G (roughly 25% of the room-temperature value). This behavior reproduces across all samples measured and is quantitatively reproduced upon temperature cycling of individual films. The abruptness of this change is distinct from the broad and monotonic behavior observed for temperatures greater than 9 K. The origin of this abrupt change is unclear, but there are two potential explanations consistent with this phenomenology. First, it is possible that the increase in strain results in an abrupt relaxation through the creation of structural defects. This explanation would require some level of self healing upon warming in order to explain the reproducibility of the transition. Given the lack of a long-range structural order in V[TCNE]_x films as-grown,³⁷ it is possible that any residual structural defects do not contribute to additional magnetic loss (damping). Second, it is possible that there exist paramagnetic spins in the system that magnetically order at temperatures below 9 K. If such spins were preferentially located in an interface layer, for example, their ordering could create an exchange bias that would then pull the easy axis back to an in-plane orientation.

The temperature dependence of the linewidth of the magnetic resonance provides an additional avenue for evaluating these potential explanations. Figure 4 shows the linewidth for the in-plane magnetic resonance from 300 K to 5 K, with additional data to more clearly resolve the sharp change between 5 K and 9 K. The linewidth data presented in Fig. 4 are extracted from a single (in-plane applied magnetic field orientation) scan. As a result, the initial dataset underlying Fig. 3 was supplemented by a second temperature dependent scan at a fixed

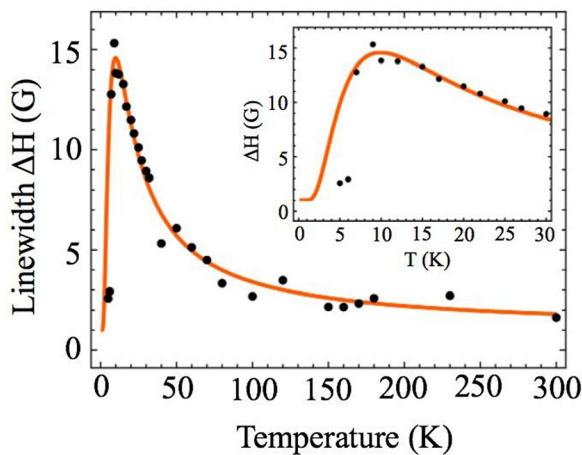


FIG. 4. V[TCNE]_x linewidth as a function of temperature (black points) and corresponding curve fit (orange line) using Eq. (4).

angle in Fig. 4. These data reveal a monotonic increase in the linewidth with decreasing temperature from 300 K down to 9 K followed by a dramatic decrease in the linewidth between 9 K and 5 K, coincident with the abrupt change in magnetic anisotropy. We note that in studies of YIG thin films broadly similar phenomenology is observed, though with a maximum in linewidth that is both higher amplitude (roughly 28 times the room-temperature value) and at higher temperature (typically 25 K) than is observed here.^{23,30} Prior work^{23,28} has explained this behavior using a model of magnon scattering from paramagnetic defect spins (also referred to as two-level fluctuators, TLF) wherein the scattering cross section at high temperature increases with decreasing temperature as the thermal polarization of the spins increases. This phenomenology competes with magnon-pumping of the paramagnetic spins into their excited state, a process that saturates as the spin lifetime of the defects becomes long relative to the spin-magnon scattering time. The competition between these two processes yields a local maximum in the damping (linewidth) that depends on the temperature dependent spin lifetime, t_s , the energy separation between majority and minority spin states, $\hbar\omega_{eg}$, and the difference between that energy splitting and the uniform magnon energy, $(\hbar\omega - \hbar\omega_{eg})$.

In this model, the linewidth expression is proportional to the square of the exchange interaction energy between V[TCNE]_x atoms and the impurity level $(\hbar\omega_{int})^2 \sim (\hbar\omega_{eg})^2$, a line shape factor accounting for the finite spin lifetime, $1/t_s / [\hbar^2/t_s^2 + (\hbar\omega - \hbar\omega_{eg})^2 t_s^2]$ and the ratio between the ground and excited impurity states for fast impurity relaxation, $\tanh(\hbar\omega/2k_B T)$,^{23,28}

$$\Delta H = \frac{S N_{imp}}{\gamma N} (\hbar\omega_{int})^2 \frac{1/t_s}{\hbar^2/t_s^2 + (\hbar\omega - \hbar\omega_{eg})^2 t_s^2} \times \tanh\left(\frac{1}{2} \frac{\hbar\omega}{k_B T}\right) + H_0, \quad (4)$$

where N_{imp}/N is the ratio between number of impurities and number of V[TCNE]_x atoms, and S is the averaged V[TCNE]_x spin per site, γ is the gyromagnetic ratio, and H_0 is a constant offset due to other relaxation mechanisms. In addition, we assume spin lifetime $t_s = t_\infty \frac{E_b}{e^{\hbar\omega_{eg}/k_B T}}$,^{31,38,39} where t_∞ is the spin lifetime limit at very high temperatures and E_b is a phenomenological activation energy. Figure 4 includes a fit of Eq. (4) to the experimental linewidth (orange line) that yields for $S \sim 1$ and $\omega_{int} \sim \omega_{eg}$ the parameters: $\omega_{eg} t_\infty = 0.98$, $E_b = 1$ meV, $\omega_{eg} N_{imp}/N = 36.5$ GHz, and $H_0 = 1$ G. Interestingly, if we assume a reasonable value for $\hbar\omega_{eg}$ of 1.3 meV, a value of $N_{imp}/N = 0.1$ follows, thus indicating that V[TCNE]_x is an exceptional low-loss magnetic material even if we assume an impurity concentration as high as 10%. This observation is consistent with the hypothesis of insensitivity to structural defects discussed above.

However, it is important to note that the peak in linewidth coincides with the abrupt reversion in anisotropy from an out-of-plane easy-axis to an in-plane easy-axis. This change in magnetic anisotropy has the potential to have a substantial impact on spin-magnon scattering efficiency. For example, this change will result in a shift of the energy of the magnon bands [see Eq. (1)], and if this change involves a commensurate change in the strain there will also be a modification to the spin-orbit coupling and exchange parameters at the paramagnetic defects. It should be noted that although this reentrant anisotropy is an intriguing feature, the fits to our model for TLFs in Fig. 4 are able

to reproduce our linewidth data without reference to this effect. As a result, we interpret this fit as an upper bound on E_b . This is represented by the additional fits shown in Fig. S7 within the [supplementary material](#) wherein we assume a lower temperature for the nominal peak in linewidth occurring due to spin-magnon scattering that is experimentally preempted by the change in magnetic anisotropy. These alternate fits agree with experimental observations at temperatures above 9 K and therefore must be considered as possible mechanisms. Moreover, if the residual paramagnetic spins are ordered at temperatures below 9 K, one would require a large amount of energy ($\gg \hbar\omega$) to populate their excited states, which is unlikely to happen. Hence, magnetic ordering of the paramagnetic spins would also enhance the suppression of spin-magnon scattering, resulting in the sharp linewidth suppression for $T < 9$ K.

When considering the expected behavior as the temperature is further reduced below 5 K, as would be the case for many applications in QISE, it is useful to consider recent millikelvin-range measurements of YIG films.⁴⁰ That work confirms the expected continued narrowing down to 500 mK followed by a modest increase from 500 mK down to 20 mK, for an overall line narrowing of roughly a factor of 2. The model of scattering from TLFs described above is consistent with this result in YIG if one supposes a second population of TLFs that are dipole coupled to the magnons rather than exchange coupled, for example, dilute magnetic impurities in the substrate or environment. We note that extending this model into $V[\text{TCNE}]_x$ requires taking into account: (i) the substantial difference in structure and chemistry between $V[\text{TCNE}]_x$ and YIG and (ii) the fact that M_s in $V[\text{TCNE}]_x$ is roughly 20 times smaller than in YIG. The former consideration indicates that the presence of these dipole coupled TLFs need not correlate between the two systems, while the latter predicts that any relaxation associated with their presence should be reduced by a factor of 20 from Ref. 40. As a result, the overall factor of 2 decrease in the linewidth observed in YIG between temperatures of 5 K and 20 mK should be taken as an extremely conservative lower bound on the performance of $V[\text{TCNE}]_x$. Given that the linewidth in $V[\text{TCNE}]_x$ at 5 K is already on par with its room temperature value, these results firmly establish the suitability for this material for applications in quantum magnonics and related aspects of QISE.

In conclusion, this work presents the first systematic study of the magnetization dynamics of $V[\text{TCNE}]_x$ at low temperatures. A strong variation in resonance frequency and anisotropy with temperature is observed and attributed to a temperature-dependent strain arising from the mismatch in thermal expansion coefficients between $V[\text{TCNE}]_x$ films and their sapphire substrates. The resonance linewidth of these films is found to increase with decreasing temperature up to a maximum value of 15 G (roughly nine times the room-temperature value) and is well fit by a model based on magnon scattering from paramagnetic defect spins. At 5 K, the magnetic anisotropy reverts to in-plane, coinciding with a nearly complete recovery of the resonance linewidth to room-temperature values; quantitative modeling suggests that the linewidth behavior arises from scattering from paramagnetic defect spins that is suppressed at very low temperature. This suppression of spin-magnon scattering is expected to strengthen as temperature is further decreased into the milli-kelvin range due to freeze-out of thermal magnons and phonons, providing a compelling case for the utility of $V[\text{TCNE}]_x$ for low-temperature microwave

applications, such as those emerging in the field of quantum information science and technology.

See the [supplementary material](#) for datasets pertaining to temperature-dependent anisotropy of the $V[\text{MeTCEC}]_x$, method for extracting linewidth of $V[\text{TCNE}]_x$ from FMR scans and additional fits to experimental data highlighting temperature dependence of the $V[\text{TCNE}]_x$ linewidth.

AUTHORS' CONTRIBUTIONS

H.Y. and M.C. contributed equally to this work.

ACKNOWLEDGMENTS

The authors would like to thank A. Franson for providing a software suite for fitting FMR spectra as well as general fitting assistance and G. Fuchs for fruitful discussions. The work presented in the main text, both experiment and theory, was primarily supported by the U.S. Department of Energy, Office of Basic Energy Sciences, under Award No. DE-SC0019250. S. Kurfman was supported by No. NSF EFMA-1741666 and grew $V[\text{TCNE}]_x$ calibration samples used for preliminary measurements not explicitly included in this paper. Work on $V[\text{MeTCEC}]_x$ presented in the [supplementary material](#) was performed by M. Chilcote and Y. Lu with the support of NSF Grant No. DMR-1741666.

DATA AVAILABILITY

The data that support the findings of this study are available within the article and its [supplementary material](#).

REFERENCES

- A. Raveendran, M. T. Sebastian, and S. Raman, *J. Electron. Mater.* **48**, 2601 (2019).
- Ü. Özgür, Y. Alivov, and H. Morkoç, *J. Mater. Sci. Mater. Electron.* **20**, 789 (2009).
- J. M. Silveyra, E. Ferrara, D. L. Huber, and T. C. Monson, *Science* **362**, eaao0195 (2018).
- Y. Tabuchi, S. Ishino, A. Noguchi, T. Ishikawa, R. Yamazaki, K. Usami, and Y. Nakamura, *Science* **349**, 405 (2015).
- E. Lee-Wong, R. Xue, F. Ye, A. Kreisel, T. Van Der Sar, A. Yacoby, and C. R. Du, *Nano Lett.* **20**, 3284 (2020).
- R. G. E. Morris, A. F. Van Loo, S. Kosen, and A. D. Karenowska, *Sci. Rep.* **7**, 11511 (2017).
- S. P. Wolski, D. Lachance-Quirion, Y. Tabuchi, S. Kono, A. Noguchi, K. Usami, Y. Nakamura, and E. Wahlström, *Phys. Rev. Lett.* **125**, 117701 (2020).
- D. Lachance-Quirion, Y. Tabuchi, A. Gloppe, K. Usami, and Y. Nakamura, *Appl. Phys. Express* **12**, 070101 (2019).
- S. Kosen, R. G. E. Morris, A. F. Van Loo, and A. D. Karenowska, *Appl. Phys. Lett.* **112**, 012402 (2018).
- D. R. Candido, G. D. Fuchs, E. Johnston-Halperin, and M. E. Flatté, *Mater. Quantum Technol.* **1**, 011001 (2020).
- V. S. Lutovinov and M. Y. Reizer, *Zh. Eksp. Teor. Fiz.* **77**, 707 (1979).
- D. Lachance-Quirion, S. P. Wolski, Y. Tabuchi, S. Kono, K. Usami, and Y. Nakamura, *Science* **367**, 425 (2020).
- R. G. E. Morris, A. F. Van Loo, S. Kosen, and A. D. Karenowska, *Sci. Rep.* **7**, 1 (2017).
- M. Kostylev and A. A. Stashkevich, *J. Magn. Magn. Mater.* **484**, 329 (2019).
- M. C. Onbasli, A. Kehlberger, D. H. Kim, G. Jakob, M. Kläui, A. V. Chumak, B. Hillebrands, and C. A. Ross, *APL Mater.* **2**, 106102 (2014).
- S. A. Manuilov and A. M. Grishin, *J. Appl. Phys.* **108**, 093713 (2010).

- ¹⁷S. A. Manuilov, R. Fors, S. I. Khartsev, and A. M. Grishin, *J. Appl. Phys.* **105**, 094102 (2009).
- ¹⁸M. Harberts, Y. Lu, H. Yu, A. J. Epstein, and E. Johnston-Halperin, *J. Visualized Exp.* **101**, e52891 (2015).
- ¹⁹H. Yu, M. Harberts, R. Adur, Y. Lu, P. C. Hammel, E. Johnston-Halperin, and A. J. Epstein, *Appl. Phys. Lett.* **105**, 012407 (2014).
- ²⁰N. Zhu, X. Zhang, I. H. Froning, M. E. Flatté, E. Johnston-Halperin, and H. X. Tang, *Appl. Phys. Lett.* **109**, 082402 (2016).
- ²¹A. Franson, N. Zhu, S. Kurfman, M. Chilcote, D. R. Candido, K. S. Buchanan, M. E. Flatté, H. X. Tang, and E. Johnston-Halperin, *APL Mater.* **7**, 121113 (2019).
- ²²C. Hauser *et al.*, *Sci. Rep.* **6**, 1 (2016).
- ²³M. Sparks, *Ferromagnetic-Relaxation Theory* (McGraw-Hill, New York, 1964), p. 226.
- ²⁴D. De Caro, M. Basso-Bert, J. Sakah, H. Casellas, J. P. Legros, L. Valade, and P. Cassoux, *Chem. Mater.* **12**, 587 (2000).
- ²⁵J. M. Manriquez, G. T. Yee, R. S. McLean, A. J. Epstein, and J. S. Miller, *Science* **252**, 1415 (1991).
- ²⁶K. I. Pokhodnya, A. J. Epstein, and J. S. Miller, *Adv. Mater.* **12**, 410 (2000).
- ²⁷I. H. Froning, M. Harberts, Y. Lu, H. Yu, A. J. Epstein, and E. Johnston-Halperin, *Appl. Phys. Lett.* **106**, 122403 (2015).
- ²⁸P. E. Seiden, *Phys. Rev.* **133**, A728 (1964).
- ²⁹A. M. Clogston, *Bell Syst. Tech. J.* **34**, 739 (1955).
- ³⁰C. L. Jermain, S. V. Aradhya, N. D. Reynolds, R. A. Buhrman, J. T. Brangham, M. R. Page, P. C. Hammel, F. Y. Yang, and D. C. Ralph, *Phys. Rev. B* **95**, 174411 (2017).
- ³¹W. A. Yager, J. K. Galt, and F. R. Merritt, *Phys. Rev.* **99**, 1203 (1955).
- ³²H. Puzkarski and M. Kasperski, *Acta Phys. Pol.-Ser. A* **121**, 1165 (2012).
- ³³M. Chilcote, M. Harberts, B. Fuhrmann, K. Lehmann, Y. Lu, A. Franson, H. Yu, N. Zhu, H. Tang, G. Schmidt, and E. Johnston-Halperin, "Spin-wave confinement and coupling in organic-based magnetic nanostructures," *APL Mater.* **7** (2019).
- ³⁴Y. Mei *et al.*, *Proc. Natl. Acad. Sci.* **114**, 33 (2017).
- ³⁵H. Suhl, *Phys. Rev.* **97**, 555 (1955).
- ³⁶J. Smit and H. G. Beljers, *Philips Res. Rep.* **10**, 113 (1955).
- ³⁷M. Chilcote, Y. Lu, and E. Johnston-Halperin, *Organic-Based Magnetically Ordered Films* (World Scientific, 2018).
- ³⁸J. K. Galt and E. G. Spencer, *Phys. Rev.* **127**, 1572 (1962).
- ³⁹H. Maier-Flaig, S. Klingler, C. Dubs, O. Surzhenko, R. Gross, M. Weiler, H. Huebl, and S. T. B. Goennenwein, *Phys. Rev. B* **95**, 214423 (2017).
- ⁴⁰S. Kosen, A. F. van Loo, D. A. Bozhko, L. Mihalceanu, R. Gross, and A. D. Karenowska, *APL Mater.* **7**, 101120 (2019).